

Estimation of potential evapotranspiration from extraterrestrial radiation, air temperature and humidity to assess future climate change effects on the vegetation of the Northern Great Plains, USA



David A. King^{a,1,*}, Dominique M. Bachelet^{a,b}, Amy J. Symstad^c, Ken Ferschweiler^b, Michael Hobbins^d

^a Biological and Ecological Engineering, Oregon State University, Corvallis, OR 97331, USA

^b Conservation Biology Institute, 136 SW Washington Ave., Suite 202, Corvallis, OR 97333, USA

^c US Geological Survey, Northern Prairie Wildlife Research Center, Wind Cave National Park, 26611 U.S. Hwy 385, Hot Springs, SD 57747, USA

^d National Integrated Drought Information System, NOAA-ESRL, Boulder, CO 80305, USA

ARTICLE INFO

Article history:

Received 18 April 2014

Received in revised form 20 October 2014

Accepted 27 October 2014

Available online xxx

Keywords:

Climate change

MC1

Great Plains USA

Potential evapotranspiration

Vegetation dynamics

ABSTRACT

The potential evapotranspiration (PET) that would occur with unlimited plant access to water is a central driver of simulated plant growth in many ecological models. PET is influenced by solar and longwave radiation, temperature, wind speed, and humidity, but it is often modeled as a function of temperature alone. This approach can cause biases in projections of future climate impacts in part because it confounds the effects of warming due to increased greenhouse gases with that which would be caused by increased radiation from the sun. We developed an algorithm for linking PET to extraterrestrial solar radiation (incoming top-of-atmosphere solar radiation), as well as temperature and atmospheric water vapor pressure, and incorporated this algorithm into the dynamic global vegetation model MC1. We tested the new algorithm for the Northern Great Plains, USA, whose remaining grasslands are threatened by continuing woody encroachment. Both the new and the standard temperature-dependent MC1 algorithm adequately simulated current PET, as compared to the more rigorous PenPan model of Rotstayn et al. (2006). However, compared to the standard algorithm, the new algorithm projected a much more gradual increase in PET over the 21st century for three contrasting future climates. This difference led to lower simulated drought effects and hence greater woody encroachment with the new algorithm, illustrating the importance of more rigorous calculations of PET in ecological models dealing with climate change.

© 2014 Elsevier B.V. All rights reserved.

1. Introduction

Climate change may affect watershed hydrology and plant water availability by altering patterns of precipitation and evapotranspiration (ET), thereby influencing the growth and survival of plants. These water-dependent effects are often related to potential evapotranspiration (PET), commonly defined as the ET of a uniform, densely vegetated area with abundant soil water in the rooting zone (Rao et al., 2011). PET has been used to calculate a variety of aridity, drought and soil moisture indices, including the ratio of precipitation to PET, precipitation–PET, PET–ET, or ET/PET. The widely used Palmer Drought Severity Index is also linked to

potential evapotranspiration (Guttman, 1998; Sheffield et al., 2012). Such PET-based indices are used (along with other climate variables) to model plant productivity (Churkina et al., 1999), drought-induced tree mortality (Gustafson and Sturtevant, 2013), the extent and frequency of wildfire (Littell et al., 2010) and the geographic ranges of plant species (Gray and Hamann, 2013).

Evaporation, and therefore PET, is influenced by incoming solar radiation, which provides the energy required to evaporate water, and aerodynamic effects dependent on wind, humidity, and temperature. These two aspects of evaporation are incorporated in the Penman formula applied to open water by Penman (1948). The approach was adapted to vegetation by Monteith (1965) in the Penman–Monteith equation, which includes the additional resistance to water vapor transfer imposed by plant stomata. These methods can provide accurate estimates of water use by irrigated crops (Howell and Evett, 2006), but have substantial data requirements, including net radiation (or a parameterization to

* Corresponding author. Tel.: +1 541 757 0687; fax: +1 541 752 0518.

E-mail address: kingda@onid.oregonstate.edu (D.A. King).

¹ Current address: 845 SW 10th St., Corvallis, OR 97333, USA.

calculate it from shortwave radiation), near-surface air temperature, vapor pressure or dewpoint temperature, and wind speed (Jensen et al., 1990). Other than temperature and vapor pressure, direct measures or station-based interpolations of these variables are not available over most of the earth, though coarse-scale estimates derived from reanalyses of station data have recently become available (Mitchell et al., 2004). Thus, more empirical methods, often reliant solely on temperature, have remained in use for estimating PET (e.g., Thornthwaite, 1948). In such methods, temperature is assumed to act as a proxy for both net radiation and vapor pressure deficit.

However, empirical approaches may differ substantially from each other in their PET predictions (Lu et al., 2005) and give rise to varying biases across geographic regions (Hobbins et al., 2008; Fisher et al., 2011). In many regions, pan evaporation, which is closely related to PET, has decreased over the 30–50 year period preceding ~2000, even though temperature has generally increased over this period. Thus, temperature-based methods may yield increases in PET that are at variance with observed trends (Roderick et al., 2009).

Temperature-based methods may be particularly prone to error when extrapolated into the future to assess the effects of greenhouse-gas driven warming on PET (Milly and Dunne, 2011). Such biases are derived from the fact that increasing temperature by increasing solar radiation would likely cause a greater increase in PET than would increasing temperature by increasing greenhouse gases, because radiation provides the energy driving evapotranspiration (Scheff and Frierson, 2014). Thus, projections of future drought severity and its effects on vegetation may be overestimated by the use of temperature-based estimates of PET derived from historical climate data. One such example of this potential for bias involves the future rate of woody encroachment of grasslands, which we consider here.

One could prevent such biases by making use of radiation outputs from the general circulation models (GCMs) used to project future climates (IPCC, 2007; Taylor et al., 2012), but the GCM outputs are at coarse scales (>100 km resolution) and must be spatially downscaled for use at the increasingly fine scales of ecological models, commonly at resolutions of 1–10 km. Methods for statistically downscaling temperature, precipitation, and water vapor pressure are readily available, based on the fine-scale spatial pattern of historical means for these variables (Fowler et al., 2007). These historical means can be derived from gridded values of historical data, such as that available from the PRISM group (Daly et al., 2008). Fine-scale gridded data for net radiation is not yet available, and this variable is seldom used in ecological assessment models. However, ground level radiation has been linked to the incoming solar radiation at the top of the atmosphere (extraterrestrial radiation), which is a function of site latitude and time of year (Thornton and Running, 1999), thereby providing an alternative method for estimating PET.

Unbiased estimates of future PET are especially important for assessing how climate change may affect semiarid ecosystems, where water substantially limits plant productivity. One such region is the Northern Great Plains, USA, which harbors exceptional and distinctive biodiversity (Olson and Dinerstein, 2002). Although more than 70% of the region's mixed-grass prairie has been converted to row-crop agriculture or otherwise developed, the region still contains more than 15 million ha of native grassland (Samson et al., 1998). Trees and shrubs have increasingly invaded the remaining Great Plains grasslands over the past century, reducing habitat for grassland specialist birds and mammals and forage production for domestic livestock (Eggemeier et al., 2006; Spencer et al., 2009; Barger et al., 2011). Climate change may accelerate or decelerate this process, depending on the direction and degree of change in temperature,

precipitation, and humidity; direct effects of increased CO₂ on productivity and water use efficiency; and fire and grazing regimes.

To assess the threat of woody encroachment in the Northern Great Plains, USA (NGP), we have used the dynamic vegetation model MC1 (Bachelet et al., 2001), which calculates monthly water balance and plant growth as limited by water and other factors. In the standard version of MC1, these calculations are based on PET determined with Linacre's (1977) algorithm, which is derived from the Penman equation, but uses semi-empirical temperature relations to estimate net radiation. This approach makes future PET estimates susceptible to bias. We therefore derived a method that reduces the potential bias in estimating net radiation from temperature alone by linking it to extraterrestrial radiation, as calculated from site latitude and time of year. We calibrated the new PET algorithm with radiation data from the NGP to assess the likelihood of woody encroachment of NGP grasslands as influenced by future climate and land management practices.

Here we compare our new PET values with gridded estimates of monthly pan evaporation synthesized by the PenPan model of Rotstajn et al. (2006) using a comprehensive set of climate and radiation inputs derived from the North American Land Data Assimilation System. Pan evaporation is a widely reported measure of evaporative demand, which can be used to approximate PET when multiplied by a factor of 0.7 (Eagleman, 1967). Next, we compare PET calculated with the new algorithm to that of the original algorithm of MC1 for three contrasting future climates, chosen for use in our assessment of woody encroachment of the NGP. We then project future woody encroachment by MC1 with the new vs. original PET algorithm for the three future climates with three fire-management scenarios. For this purpose we used the MC1 version of King et al. (2013a,b); King et al. (2013a,b) that was calibrated for the ponderosa pine (*Pinus ponderosa*)–grassland ecotone at Wind Cave National Park in the southern Black Hills of South Dakota, which lie within the larger NGP region. For the current projections we further calibrated MC1 for *Juniperus virginiana* (eastern redcedar), a native tree that has been particularly invasive of grasslands of the SE portion of the NGP and with future warming may threaten much of the NGP, and for *Juniperus scopulorum* (Rocky Mountain juniper), which is encroaching into grasslands in the western portion of the NGP.

2. Materials and methods

Our approach takes the following steps:

1. Determine an empirical relation for atmospheric transmittance of solar radiation as a function of monthly maximum and minimum temperatures (T_{max}, T_{min}), where transmittance = monthly shortwave insolation on a horizontal surface/monthly extraterrestrial insolation.
2. Use Linacre's (1968) approach to estimate net radiation from mean monthly temperature and solar irradiation (i.e., transmittance × extraterrestrial insolation).
3. Use net radiation (Q_n) and Linacre's (1977) approximations of the relevant properties of air and water vapor in the Penman equation to derive an algorithm relating PET to mean monthly values of Q_n , temperature and dewpoint temperature.
4. Compare our estimates of historical monthly PET for the NGP with those of the standard MC1 PET algorithm and the synthetic pan evaporation estimates of Hobbins et al. (2012), which were multiplied by 0.7 to approximate PET. Hobbins and co-workers' estimates involve additional inputs and processes, such as wind speed, not included in our algorithm.
5. Compare our estimates of PET for the NGP with those of the standard PET algorithm of MC1 using future climate variables

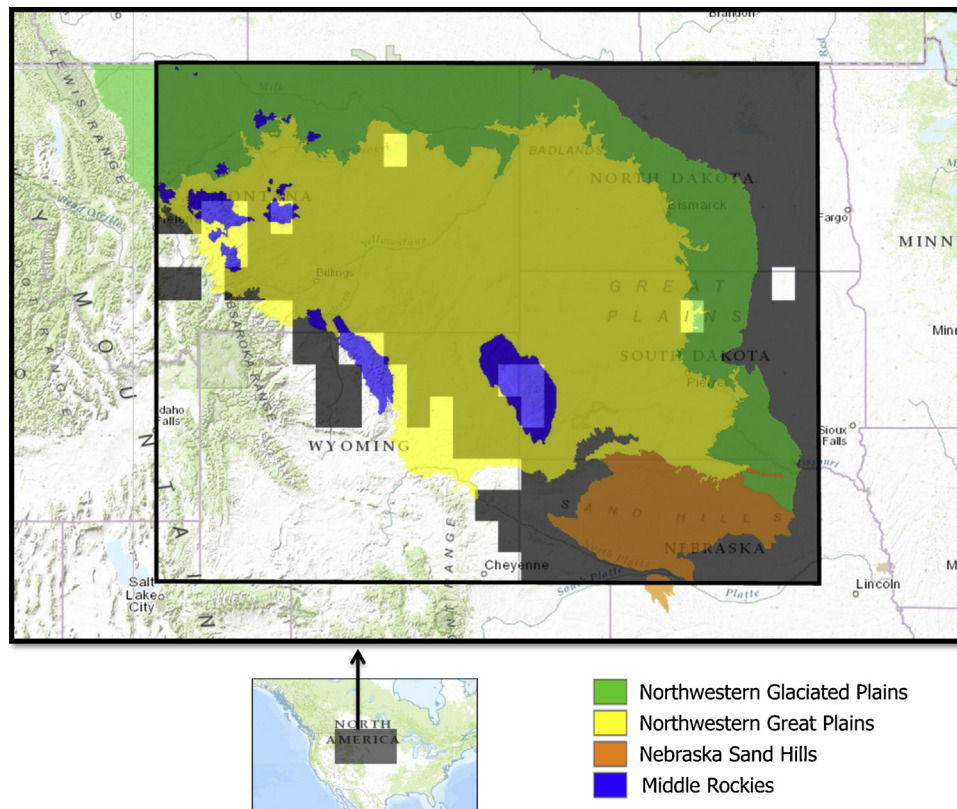


Fig. 1. Northern Great Plains study area shown in gray in the upper panel. U.S. Northern Great Plains shown in color. Two eastern cells and a north-central cell (shown as blanks) were excluded for lack of soil data. Other cells, mostly in the southwest corner of the grid, were excluded for being >1500 m elevation. (For interpretation of the references to color in this figure legend, the reader is referred to the web version of this article.)

from three GCMs spanning a substantial range in temperature and humidity.

6. Compare simulations of future juniper invasion of the NGP by MC1, based on the new vs. standard PET algorithms, to assess some of the ecological implications of our revised algorithm.

2.1. Study area

For our purposes, the NGP includes the Northwestern Glaciated Plains, Northwestern Great Plains, and Nebraska Sand Hills US EPA Level III ecoregions (<http://www.epa.gov/wed/pages/ecoregions.htm>) and the lower-elevation portions of the Middle Rockies ecoregion they surround. For logistical convenience we consider a grid of 30" (~800 m) cells, each cell centered on a larger cell of arc angle 0.5° (~50 km), over the area from 41–49° N latitude and 97.5–112° W longitude. When cells of elevation >1500 m are excluded (see Section 2.5), this grid approximates our ecoregion-defined NGP (Fig. 1).

2.2. Atmospheric transmittance

Daily extraterrestrial insolation (in $\text{J m}^{-2} \text{ day}^{-1}$) was calculated following [Bristow and Campbell \(1984\)](#), as

$$Q_0 = \frac{86400S_0(h\sin\varphi\sin\delta + \cos\varphi\cos\delta\sin h)}{\pi} \quad (1)$$

where S_0 is the solar constant (1360 W m^{-2}), h is the half day length (half the time the sun is above the horizon: $\cos h = -\tan \varphi \tan \delta$), φ is site latitude and δ is the solar declination. Solar declination, latitude and half daylength are in radians.

The fraction of extraterrestrial insolation that reaches level ground as short wave radiation (transmittance) has been empirically related to daily diurnal temperature range (DTR) ([Bristow and Campbell, 1984](#)), as well as vapor pressure, and rain occurrence ([Thornton and Running, 1999](#)). However, MC1 uses monthly climate data, and the algorithms developed with daily data do not readily convert to monthly data. We therefore derived a transmittance–temperature relationship from the monthly short-wave solar irradiances of the Solar and Meteorological Surface Observation Network (SAMSON) data base ([NREL, 1993](#)). For this purpose we chose nine SAMSON stations distributed relatively evenly across the NGP ([Table 1](#)), excluding several where nearby mountains to the east and/or west may reduce direct beam irradiance. The data were from 1961 to 1990 (a slightly shorter period for two stations, [Table 1](#)).

Table 1

SAMSON stations used to estimate the relation between monthly transmittance and diurnal temperature range (DTR) for the Northern Great Plains, USA. Data for 1961–1990, except where indicated otherwise.

Station	N. latitude	Longitude	Elevation (m)
North Platte, NE	41.13	–100.68	849
Bismarck, ND	46.77	–100.75	502
Minot, ND ^a	48.27	–101.28	522
Pierre, SD	44.38	–100.28	526
Rapid City, SD	44.05	–103.07	966
Casper, WY	42.92	–106.47	1612
Sheridan, WY	44.77	–106.97	1209
Miles City, MT ^b	46.43	–105.87	803
Lewistown, MT	47.05	–109.45	1264

^a 1961–1988.

^b 1961–1989.

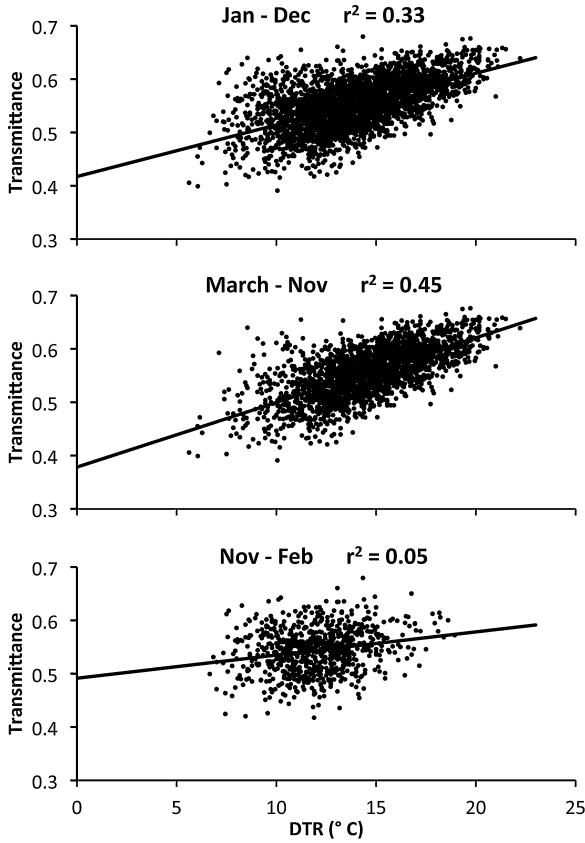


Fig. 2. Monthly transmittance (shortwave surface insolation/extraterrestrial insolation) vs. mean daily temperature range per month (DTR) for 1961–1990 at nine SAMSON stations within the NGP.

Monthly transmittance (tr) and monthly mean DTR are positively correlated, more strongly so for March through November than for December through February (Fig. 2). The weak relationship in winter likely occurs because snow cover increases transmittance under cloudy conditions, due to multiple reflections between high-albedo snow and clouds (Thornton and Running, 1999). We use the regression relation

$$tr = 0.37830(\pm 0.0041sd) + 0.012125(\pm 0.00028)DTR \quad (2)$$

derived from the 2403 monthly values for March through November to match our emphasis on the growing season. Short-wave insolation (Q_s) can then be calculated as

$$Q_s = trQ_0 \quad (3)$$

2.3. Net radiation

Linacre (1967, 1968,) derived the following linear approximation for net radiation (Q_n) by assuming that outgoing long-wave radiation is that which would be emitted when ground temperature equals near-surface air temperature and the ground emissivity is 1:

$$Q_n = (1 - \alpha)Q_s - 1440 \times 0.16F(1 - 0.01T) \quad (4)$$

where α is surface albedo, $F = 0.2 + 0.8(n/N)$, where n/N is the fraction of daylight hours with bright sunshine, and T is the mean temperature ($^{\circ}C$) over the period for which Q_n is calculated. Both Q_n and Q_s are in $cal\ cm^{-2}\ day^{-1}$, i.e., the numeric value of Q_s in Eq. (3) has been multiplied by 0.000239 to convert it to these units 2.

(We use the original units of Linacre (1968, 1977,) in our derivation, thereby retaining the one or two significant digits of his approximated coefficients and convert our final expression for PET to standard metric units.) Based on relations between diffuse and direct short-wave radiation and atmospheric transmittance (tr) reported by Spitters et al. (1986), we assume that the sunlit fraction n/N increases linearly with the transmittance (tr), ranging from 0 for $tr \leq 0.25$ to 1 when $tr \geq 0.75$. Thus,

$$F = 0.2 + \frac{0.8(tr - 0.25)}{0.5} \quad (5)$$

which is floored and capped at 0.2 and 1, respectively. Following Linacre (1977) we set $\alpha = 0.05$, the albedo of open water. Because Q_n varies linearly with T , Eq. (4) should yield relatively unbiased estimates when monthly means are used for temperature and Q_s .

2.4. Calculation of PET based on net radiation and air and dewpoint temperatures

Linacre (1977) expressed the Penman formula for evaporation from open water as

$$L \times PET_0 = \left[\frac{Q_n + \rho c S / \Delta r_a}{1 + \gamma / \Delta} \right] \quad (6)$$

where L is the latent heat of vaporization of water ($\cong 580\ cal\ g^{-1}$), PET_0 is potential evaporation from open water in $g\ cm^{-2}\ s^{-1}$, ρ is the density of air ($\cong 0.0013\ g\ cm^{-3}$), c is the specific heat of air ($\cong 0.24\ cal\ g^{-1}\ ^{\circ}C^{-1}$), S is the vapor pressure deficit (mbar), Δ is the derivative of saturation vapor pressure with respect to air temperature ($mbar\ ^{\circ}C^{-1}$), and γ is the psychrometric constant ($mbar\ ^{\circ}C^{-1}$). Here r_a is the momentum surface aerodynamic resistance, which decreases with increasing wind speed, set to an intermediate value of $1.2\ s\ cm^{-1}$ by Linacre (1977). The expressions $1 + \gamma / \Delta$ and S / Δ were approximated in terms of temperature and dewpoint temperature (T_d) by Linacre (1977) as:

$$1 + \frac{\gamma}{\Delta} = 2 - 0.025T \quad (7)$$

and

$$\frac{S}{\Delta} = (T - T_d) \quad (8)$$

where both temperatures are in $^{\circ}C$. These estimates are within 10% of actual values over a temperature range of 8–36 $^{\circ}C$ (Linacre, 1977). They are reasonable for an approach based on monthly averaged inputs and with substantial uncertainties due to the lack of wind speed data.

Converting Q_n from Eq. (4) to $MJ\ m^{-2}$ and substituting these approximations into Eq. (6) and expressing PET_0 in $mm\ day^{-1}$ yields

$$PET_0 = \frac{23.9Q_n}{58(2 - 0.025T)} + \frac{15(T - T_d)}{80 - T} \quad (9)$$

where monthly averages are used for T , T_d and Q_n . The right hand term of Eq. (9) is identical to the right hand term of Linacre's (1977) expression for PET_0 , but our expression for Q_n (Eq. (4)) is linked to extraterrestrial insolation and temperature rather than to temperature alone.

We follow the convention used in MC1 of adjusting PET_0 by a user-specified scalar, set to 0.9, because the potential evapotranspiration from an herbaceous canopy transpiring without limitation by soil water is typically somewhat less than the evaporation from open

water. We also set $PET = 4.5 \text{ mm month}^{-1}$ if the calculated value falls below this value, as done in the standard MC1 PET algorithm, with the rationale that months that are on average cold and dark will nonetheless include some brighter, warmer intervals of positive PET. Hence,

$$PET = \max(0.9PET_0, 4.5) \quad (10)$$

In addition, we replaced Linacre's (1977) temperature-based estimate of dewpoint temperatures with available values for the historical simulation, or vapor pressure converted to dewpoint temperature for the future simulations by MC1. This approach permits direct comparison of PET values generated by MC1 with the new algorithm with those of the standard temperature-related algorithm.

Thus, we have derived a method that should be more accurate for approximating monthly PET, which serves as an upper bound for the actual ET simulated by MC1 and other (but not all) process-based vegetation models. The input variables are latitude (used in calculating monthly extraterrestrial radiation), monthly mean dewpoint temperature and monthly maximum and minimum temperatures (used to calculate monthly mean temperature and diurnal temperature range). The linkage of net radiation to extraterrestrial radiation in the Penman formulation of PET is expected to substantially improve our simulations of future PET, as compared with that generated by algorithms based only on temperature.

2.5. Comparison of PET with modeled pan evaporation

We compared our simulated PET values with simulated pan evaporation generated by the PenPan model of Rotstayn et al. (2006). This model uses the Penman formulation, modified to account for the geometry of U.S. class-A evaporation pans, which are set above the ground surface and have sides that intercept additional radiation. The model was driven by seven meteorological and radiation drivers from the North American Land Data Assimilation System, as follows: 2-m air temperature and specific humidity, surface pressure, zonal and meridional components of 10-m wind speed (transformed to a 2-m height), downwelling shortwave radiation and downwelling longwave radiation. Monthly pan evaporation from the PenPan model for the May–October warm season was highly correlated with that reported from 251 pans across the U.S. ($r^2 = 0.756$), with little bias (Hobbins et al., 2012).

For our comparisons, we used monthly PenPan values for a rectangular grid of $1/8^\circ$ cells covering $41\text{--}49^\circ$ latitude, -112 to -97.5° longitude, a region including nearly all of our NGP study area. We simulated PET with our new algorithm and with the standard MC1 algorithm using a regular sampling of $30''$ climate data from the PRISM group (Daly et al., 2008), taken across the above grid at a spacing of 0.5° in latitude and longitude. Soil bulk density, depth, and texture data from Kern (1995, 2000) were downscaled to the $30''$ grid of the climate data. Soil data are not necessary to calculate PET alone, but are a required input to MC1 and were used in simulating woody encroachment (Section 2.7). We multiplied the pan evaporation values of Hobbins

et al. (2012) by 0.7, the approximate ratio of PET to U.S. class-A pan evaporation (Eagleman, 1967; Allen and Crow, 1971) and compared each PET value with the corresponding adjusted pan evaporation value for the closest $1/8^\circ$ cell centered to the NW of the PET cell. We restricted our analysis to cells of elevation $<1500 \text{ m}$ (75% of the cells) because Linacre's (1977) approximate values for the density of air and the so-called psychrometric constant are for low elevations. (These values vary with elevation in the PenPan model.) The excluded cells were mostly in the Wyoming basin and Rocky Mountains ecoregions, outside of our area of interest. The resulting grid has a natural vegetation cover that is mostly grassland (Küchler, 1975), simplifying the interpretation of our subsequent simulations of vegetation based on the two PET algorithms. With the exclusion of elevations $>1500 \text{ m}$ and three cells with missing soil data, our comparison included 343 locations over 372 months (1979–2009), the period of overlap of the pan evaporation and the PRISM climate data.

2.6. Future climate projections for PET algorithm comparisons

Twenty-first century climate projections were acquired for three GCMs that span much of the range in temperature increases associated with the IPCC SRES A2 greenhouse gas emission scenario for the conterminous US (Nakićenović and Swart, 2000): CSIRO Mk3 (Gordon, 2002), Hadley CM3 (Johns et al., 2003) and MIROC 3.2 medres (Hasumi and Emori, 2004) (henceforth CSIRO, Hadley and MIROC). GCM future projections were downscaled using the delta or anomaly method, a simple statistical approach (Fowler et al., 2007). For each climate variable and each future month, we calculated anomalies between future and mean monthly historical (1971–2000) GCM-simulated values for each GCM grid cell over the conterminous U.S. We used differences for temperature and ratios for precipitation and vapor pressure (capped at a maximum ratio of five). Anomalies were then downscaled to our $30''$ grid using bilinear interpolation and applied to the monthly historical PRISM baseline (1971–2000) available at the same spatial scale.

The three chosen GCM simulations diverge over the 21st century for the NGP (Table 2). The Hadley and MIROC futures become substantially hotter than does CSIRO. Spatially averaged annual precipitation is unchanged for Hadley, increases for CSIRO and decreases for MIROC. Relative humidity increases somewhat for CSIRO, but decreases for Hadley and especially MIROC (Table 2). There is also an increase in aridity from east to west-of-center of the NGP for both the historical and the future climates (Fig 3). CSIRO is wetter and MIROC drier than historical across the NGP. Moreover, the relative pattern of change from 1981–2000 to 2081–2100 differs among the future climates. The percent difference in precipitation is greatest in the north-central NGP for CSIRO (+44%), ranges between -15% and $+15\%$ for Hadley, and exhibits the greatest difference in the southeast NGP for MIROC (-28%).

2.7. Ecological assessment of the new PET algorithm with MC1

The dynamic global vegetation model MC1 simulates plant growth and biogeochemical cycles, vegetation type, wildfire, and

Table 2

Mean annual values over the NGP grid for 2081–2100 for downscaled climates from three GCMs (2081–2099 for Hadley). Change in comparison to the respective means for the 1981–2000 PRISM historical climate.

Future climate	Mean temperature ($^\circ\text{C}$)	Temperature change	Mean precip. (mm/yr)	Percent precip. change	Mean RH (%)	Percent RH change
CSIRO	11.06	3.92	541	23.9	65.8	9.4
Hadley	13.17	6.02	433	-0.8	58.0	-3.7
MIROC	13.78	6.63	353	-19.2	53.1	-11.7

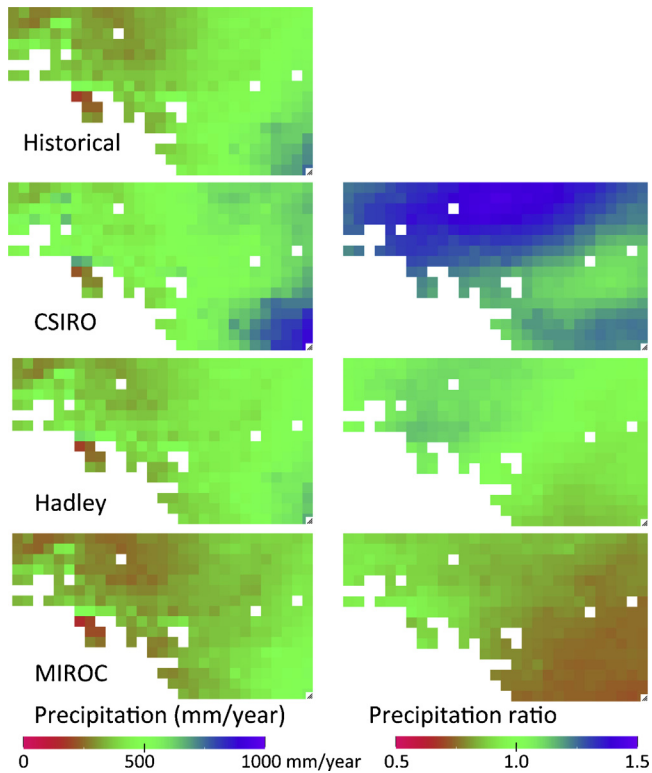


Fig. 3. Pattern of mean annual precipitation across the NGP for 1981–2000 (historical) and 2081–2100 for the indicated future climates (2081–2099 for Hadley) shown on the left. Ratio of corresponding future to historical precipitation shown on the right.

their interactions. The model simulates competition between trees and grasses (including other herbaceous species), as affected by differential access to light and water, and fire-caused tree mortality (Bachelet et al., 2000, 2001). MC1 has been used extensively to assess future climate change effects on natural vegetation and carbon stocks (Bachelet et al., 2003; Lenihan et al., 2008; Rogers et al., 2011; Halofsky et al., 2013).

Grass and tree production rates are based on maximum monthly production rates that are multiplied by temperature-, water-, and CO_2 dependent scalars that differ between grasses and trees (Bachelet et al., 2001). The water scalar ranges between 0 and 1 and is a function of the ratio of plant available water to PET, where plant available water includes monthly precipitation plus plant-extractable water in the soil layers accessed by grasses or more deeply rooted trees. Because PET is in the denominator of the water scalar function, higher estimates of PET will reduce simulated production for specified values of monthly precipitation and plant extractable water. Changes in the PET algorithm will also affect simulated transpiration, thereby affecting the rate at which plant extractable water declines during drought periods. For the simulation of natural fires, ignitions occur when temperature- and humidity-related fire danger indices are exceeded. Although PET does not affect the timing of fires, it indirectly affects simulated fire intensity and resultant tree mortality, via its effects on productivity and hence fuel loads and tree size.

MC1 projects the dynamics of lifeforms, including evergreen and deciduous needleleaf and broadleaf trees, as well as C3 and C4 grasses. However, the model can also be parametrized for a particular dominant species of the associated lifeform. Here we modified the version of MC1 of King et al. (2013a), which was calibrated to project the observed ecotone between ponderosa pine and grasslands at Wind Cave National Park in the Black Hills of South Dakota, near the center of the NGP region. Several

parameters were modified to simulate *Juniperus* rather than ponderosa pine, based on the aboveground net primary productivity and biomass reported by Norris et al. (2001) for dense stands of *J. virginiana* in NE Kansas ~200 km south of the SE corner of the NGP region considered here. The parameter KLAI, the tree stem biomass at which the leaf area index (LAI) attains half its maximum value (when leaf biomass is adequate), was reduced from 2000 to 1000 g C m^{-2} for the evergreen needleleaf lifeform that includes junipers. This change increases the LAI associated with a specified tree biomass by a factor of up to two when that biomass is low, but has little effect at high biomass. Our rationale for this change is that it better simulates the observations of Norris et al. (2001). The widespread dispersal of juniper seeds by birds should result in high densities of young junipers between existing trees, thereby substantially increasing regional LAI without a large increase in supporting woody biomass. In addition, the mortality rates for live large wood (\approx tree stems) and structural roots were increased by a factor of 1.5 for the evergreen needleleaf lifeform, for this rather small tree species.

We used the original fire mortality function of MC1 rather than that of King et al. (2013a,b); King et al. (2013a,b), which had been selected for fire-resistant ponderosa pine. We lowered the ratio of bark thickness to stem diameter (which affects fire mortality) to 0.025, the value used for Rocky Mountain juniper (*Juniperus scopularum*) by Lutes and Robinson (2003). We also halved the fuel depth ratio from 0.042 to 0.021 for the evergreen needleleaf woodland and forest vegetation types, thereby doubling the fuel packing ratio and substantially reducing the intensity and fire-caused mortality of simulated fires for these tree-dominated vegetation types. This change was made because juniper litter is somewhat less dense than that of other conifers, such as ponderosa pine and the litter of small-needled species, such as juniper, burns less intensely than that of longer needled pines (de Magalhães and Schwilk, 2012). The resultant decrease in fire intensity is consistent with observations that juniper stands suffer less fire mortality once they become dense enough to shade out the grasses, which fuel hotter fires (Fuhlendorf et al., 1996).

MC1 is run in four successive phases: an equilibrium phase, which initializes the carbon pools and vegetation types, followed by three transient phases; spinup, historical, and future. The spinup phase is run iteratively with detrended historical climate data to readjust the carbon pools and vegetation types in response to dynamic fire and the historical phase is run with transient historical climate data starting in 1895. For our assessment of the influence of the PET algorithm on woody encroachment of the NGP, we altered this protocol by setting fires every five years during the spinup and historical phases, thereby ensuring extremely low tree biomass ($0.001\text{--}0.005 \text{ g C m}^2$) across the NGP at the beginning of the future simulations. This initialization to grassland allows one to assess the effects of variation in climate across the NGP on simulated woody encroachment. To some degree this approach also accounts for the frequent grassland fires set by Native Americans before Euro-American settlement and the low frequency of firebreaks over the extensive flatter portions of the NGP that resulted in large burn areas per ignition (Higgins, 1986; Anderson, 1990; Courtwright, 2011).

We used the same future climates and sampling of every 60th $30''$ grid cell (0.5° spacing) as for the PET comparisons. We assumed that grazing animals (domestic and/or wild) remove 50% of the monthly aboveground grass production during the growing season, i.e., an intermediate grazing intensity (Holecheck et al., 1999; King et al., 2013b). This grazing level results in lower standing grass biomass and hence less intense fires than the no grazing case. Three idealized fire scenarios were chosen, based in part on our survey of land managers in the NGP: no fire; spring (May 1) fires set at 40 year intervals; and fall (Oct. 16) fires set at

Table 3

Summary statistics for the comparison of PET generated by the new algorithm (PET_{new}) and the standard algorithm ($PET_{standard}$) to that generated by the PenPan model. The first (left-hand) column indicates the comparison being made; the second column lists the ratios of mean 1979–2009 PET for the NGP (e.g., $PET_{new}/PenPan$); the third and fourth columns list the regression slopes (standard deviations in parentheses) and correlations, respectively, for annual PET per year per grid cell; the fifth column lists the correlations for the 31-year mean annual PET per grid cell; the sixth column lists the correlations for mean annual PET for the NGP. The bottom row lists the number of PET values per algorithm being compared (N). Columns 5 and 6 are based on the same data as Figs. 4 and 5, respectively.

Comparison	Ratio of mean PET	Regression slope (annual PET per year per cell)	r (annual PET per year per cell)	r (31-year mean annual PET per cell)	r (mean annual PET over NGP)
PET_{new} vs. PenPan	0.994	0.888 ± 0.0075	0.755	0.735	0.943
$PET_{standard}$ vs. PenPan	1.063	0.807 ± 0.0085	0.676	0.625	0.816
N	1 (31-year mean for the NGP)	10633 (31 years \times 343 locations)	10633 (31 years \times 343 locations)	343 locations	31 (31 years \times 1 location)

10 year intervals. The first scenario provides the simplest assessment of the effect of PET algorithm on the simulation of woody encroachment, and may apply to the subset of naturally vegetated lands that remain unburned due to successful fire suppression or chance, as influenced by landscape fragmentation. The second and third scenarios are indicative of the possible outcomes of minimal vs. more aggressive use of fire to maintain grasslands, and illustrate how fire and PET interact to affect the course of woody encroachment simulated by MC1.

3. Results and discussion

3.1. Comparison of historical PET estimates

The 31-year mean PET values for the whole NGP derived by the new and standard PET algorithms (PET_{new} and $PET_{standard}$, respectively) and the PenPan model are similar to each other, i.e., their ratios are close to one (Table 3). The correlation between annual values per grid cell for PET_{new} vs. PenPan is higher than the correlation for $PET_{standard}$ vs. PenPan and the corresponding regression slope for the former comparison is also closer to 1 than for the latter (Table 3). Annual PET is instructive for evaluating the algorithms because it integrates over the seasonal cycle and is representative of the evaporative demand faced by plants, as PET is highest during the warmer, brighter months of the growing season.

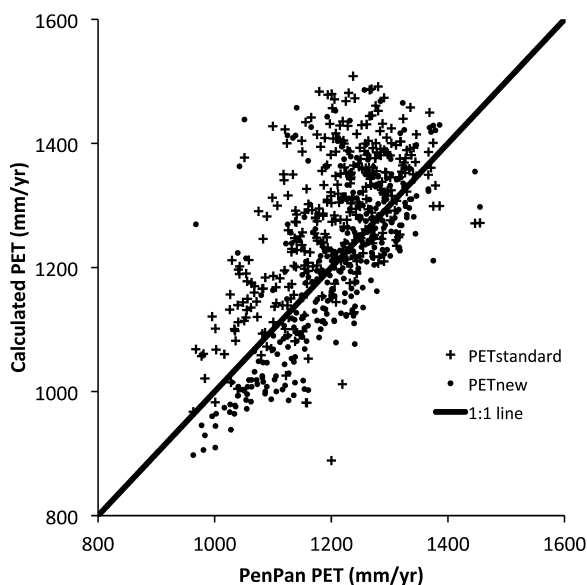


Fig. 4. Comparison of mean (1979–2009) annual PET generated by the new and standard MC1 algorithms, plotted against that of the PenPan model for each grid cell of elevation <1500 m.

The 31-year mean annual PET values per grid cell derived with our algorithms show slightly lower correlations with those of the PenPan model than for the annual values (Table 3, Fig. 4). However, annual PET for the whole NGP shows similar year-to-year variation for all three methods, with high agreement between our new algorithm and the PenPan model (Fig. 5, Table 3). All three approaches project particularly high PET for 1988, one of the most severe drought years of the 20th century for the NGP (Sud et al., 2003). The 31-year trends in PET for the NGP are relatively similar among methods and not significantly different from zero (regression slope = 0.14 ± 1.57 , -1.45 ± 1.35 and -1.18 ± 1.81 mm yr⁻¹, for PenPan PET_{new} and $PET_{standard}$, respectively, derived from the data of Fig. 5).

Thus, the new algorithm, involving extraterrestrial radiation plus monthly means of maximum and minimum temperature and dewpoint temperature, captures the year-to-year variation in PET, as calculated with the more physically rigorous PenPan model. A caveat to this conclusion is that it applies to a region within the conterminous US where temperature determined most of the variability in the annual pan evaporation projected by the PenPan model (Fig. 7 in Hobbins et al., 2012).

3.2. Comparison of future PET estimates

The spatially averaged annual PET values projected by the new vs. standard algorithms differed only slightly at the beginning of the 21st century, but diverged substantially by the end of this century for all three future climates (Table 4, Fig. 6). This divergence is associated with the 131% increase in atmospheric CO₂ concentration over the 21st century under the A2 emissions scenario used to drive the GCMs. Substantially smaller increases in PET were calculated with the new algorithm throughout the NGP (Figs. 7 and 8). For the milder CSIRO climate, the new algorithm produced 1/4 of the PET increase of the standard one (Table 4). The

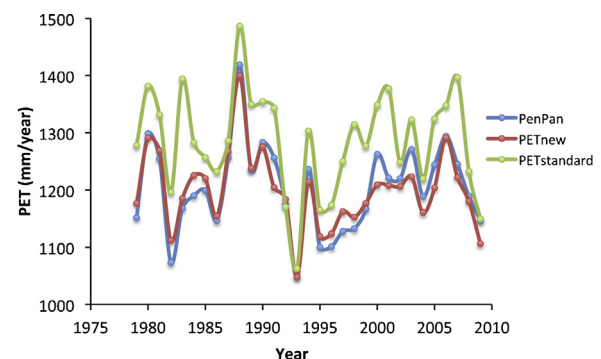


Fig. 5. Comparison of annual PET averaged over Northern Great Plains grid cells of elevation <1500 m.

Table 4

Comparison of projected mean annual PET over the NGP domain for 2081–2100 for three future climates (2081–2099 for Hadley). The percent increase is in comparison to the mean historical PET for 1981–2000 derived with the same method as used for the future projection. The range (in parentheses) gives the minimum and maximum percent increase for individual grid cells.

Future climate	PET _{standard} (mm/yr)	Percent increase (range)	PET _{new} (mm/yr)	Percent increase (range)
CSIRO	1682	31.5 (25.2 – 43.0)	1284	7.3 (2.7 – 11.3)
Hadley	2160	68.9 (55.8 – 81.5)	1619	35.3 (23.7 – 51.8)
MIROC	2168	69.5 (56.6 – 79.7)	1737	45.1 (27.6 – 63.8)

new algorithm projected half of the increase of the standard one for the hot Hadley climate, and 2/3 of the increase of the standard one for the increasingly hot and dry MIROC climate (Table 4).

These results highlight the substantial differences that exist between the three climates (Table 2). The average temperature increase over the 21st century for CSIRO is slightly less than 2/3 of that for Hadley and MIROC. This moderate increase in temperature coupled with an increase in relative humidity (RH) yields only a minor increase in PET, as calculated with the new algorithm. The late 21st century MIROC climate is only slightly warmer than the Hadley climate, but the differences in RH between the two are substantial. The new algorithm includes vapor pressure in the aerodynamic term of the Penman equation rather than inferring it from the temperature regime, as done in the standard algorithm. This change in the calculation of PET results in greater differentiation of the projected PET rise associated with the three future climates.

Our projections with the new algorithm are similar to those of Scheff (2011) who applied the Penman–Monteith equation to climate output from the MIROC3.2 medres GCM (A2 emissions scenario) that also included wind speeds and the daily energy fluxes contributing to net radiation. For the GCM grid cells overlying our NGP grid, Scheff (2011) reported PET increases of approximately 25 to 53% (mean of 38%), for the period of 2081–2100 vs. 1981–2000, similar to our mean increase of 45%

for the same GCM and emissions scenario (Table 4). The recent analysis of Scheff and Frierson (2014), based on 3-h resolution outputs of temperature, vapor pressure, wind, and radiation from 13 CMIP5 GCMs, yielded mean PET increases of 17.8% and 24.4% for lands at 15–40° N and 40–80° N, respectively, for the period of 2080–2099 vs. 1980–1999. Feng and Fu (2013) projected increases in PET of 15–20% over most of our NGP grid for 2071–2100 relative to 1961–1990, based on CMIP5 data from 27 GCMs under the RCP85 scenario.

Modest increases in PET with increasing temperature were also calculated by Morgan et al. (2011) using the American Society of Civil Engineers standardized evapotranspiration equation, driven by observed weather and solar radiation data from their experimental site adjacent to Casper WY, which is west of the south-central corner of our grid (Fig. 1). For the April 1–Oct 16 growing season over three successive years, they calculated an increase in PET of 2.6% per °C increase in temperature above ambient with ambient relative humidity, and an increase of 4.9% per degree increase in temperature with ambient vapor pressure, i.e., declining relative humidity with increasing temperature above ambient. These temperature sensitivities of PET are substantially lower than those calculated by the widely used empirical algorithm of Hamon (1961). For a 1° increase in temperature the Hamon method projects an increase in PET of 6.4%; for a 6° increase, 45%, i.e., 7.5% per degree, the larger value deriving from the exponential form of the Hamon algorithm.

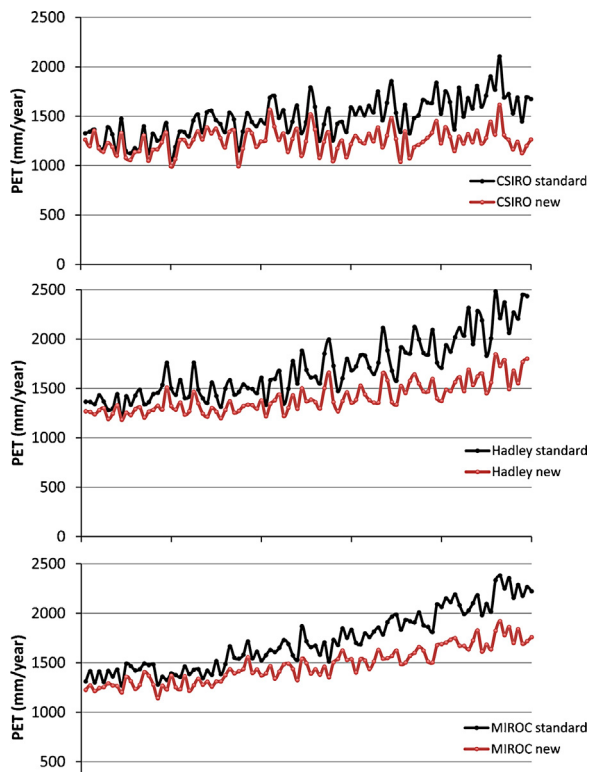


Fig. 6. Mean annual PET averaged over the NGP grid, as calculated by the new vs. standard algorithms for three downscaled GCM-derived future climates.

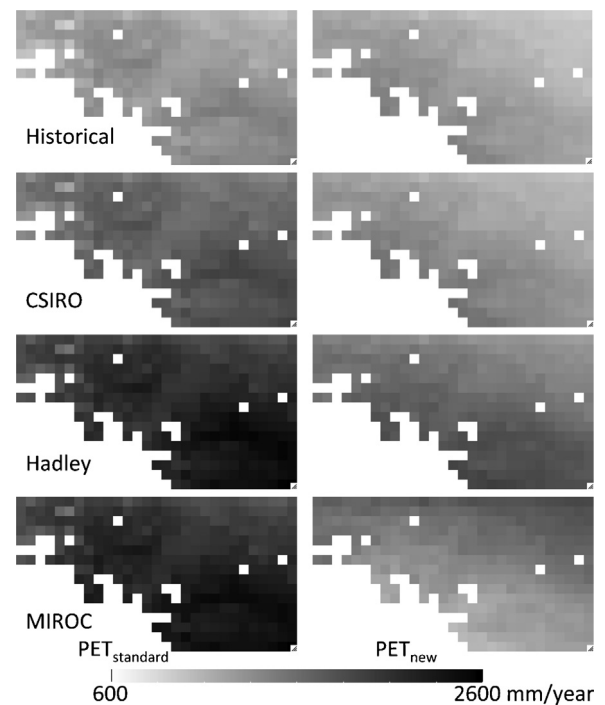


Fig. 7. PET calculated with the standard (left-hand side) and new (right-hand side) algorithms for the NGP during the historical period (1981–2000 PRISM climate) and the three future climates for 2081–2100 (2081–2099 for Hadley). (See Fig. 1 for geographic location of the grid.)

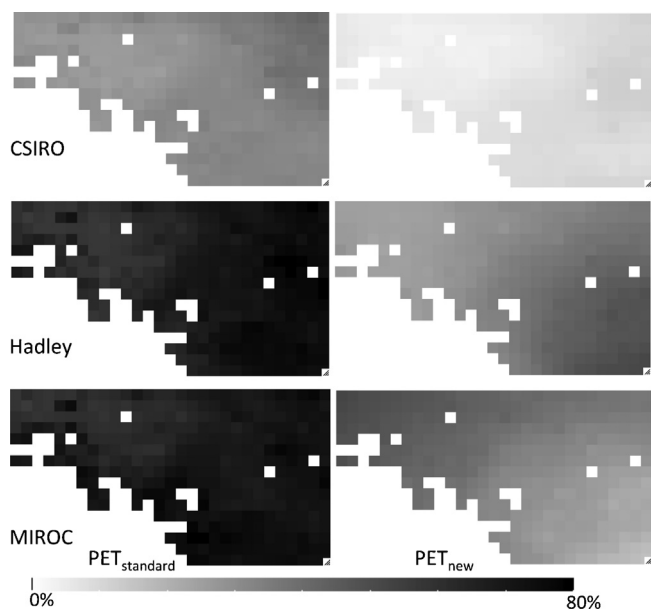


Fig. 8. Percent increase in PET across the NGP for 2081–2100 future climates vs. 1981–2000 historical climate calculated with the standard and new algorithms.

The mean PET and temperature values for our 100-year comparison (Tables 2 and 4) yield overall PET increases as calculated with the new algorithm of 1.9% (CSIRO), 5.9% (Hadley) and 6.8% (MIROC) per °C increase in mean temperature. These sensitivities are associated with an increase in mean RH (CSIRO), a

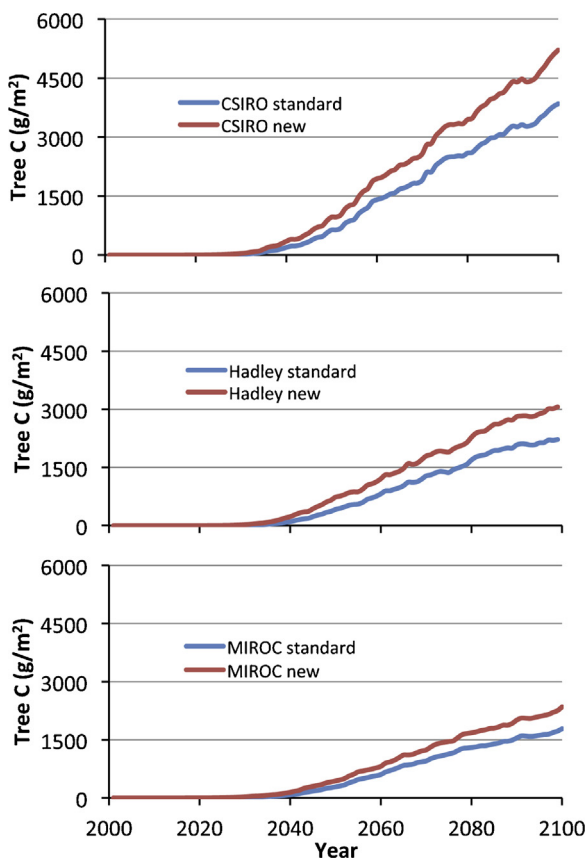


Fig. 9. Spatially averaged annual live aboveground tree C with no future fires, simulated by MC1 for the NGP with the new and standard PET algorithms for three future climates.

small decrease in RH (Hadley) and a larger decrease in RH with a small increase in mean vapor pressure (MIROC)—sensitivities unlikely to be captured by empirical algorithms for PET based only on temperature. Furthermore, these increases in future PET, achieved by linking net radiation to extraterrestrial radiation, are in better agreement with more rigorous calculations of PET from GCMs or temperature-adjusted ambient weather data than estimates derived from temperature alone.

3.3. Influence of PET on projections of woody encroachment in the Northern Great Plains

After initializing vegetation cover to grassland, the MC1 model simulates an increase in woody biomass that becomes increasingly apparent in the last several decades of the 21st century, for the no-fire case (Fig. 9). This slow appearance of woody plants is due to the very low initial woody biomass and low initial invasion capacity, as parametrized for the NGP. The overall increase and the difference in increase between the standard and new PET algorithms are greatest for the CSIRO climate and least for the MIROC climate (Fig. 9).

Large spatial variation occurs in the simulated progression of woody encroachment across the NGP for each of the six PET × climate cases. This pattern is indicated by the woody biomass attained in the 2090s for the no-fire case (Fig. 10). For each future climate, tree biomass is high near the eastern boundary, where precipitation is generally highest (Fig. 3, left column). In nearly all cases tree biomass is quite low in northeastern and north-central Montana (northwestern quarter of the study region, Fig. 10), where precipitation tends to be low and PET is relatively high (Figs. 3 and 7). This more-or-less treeless area is substantially smaller for the new PET algorithm than the standard one for each of the three future climates and scarcely exists for the milder CSIRO climate when the new PET algorithm is used. Thus, the overestimation of PET by the standard algorithm leads to the simulation of more extreme drought conditions and hence the underestimation of woody encroachment rates.

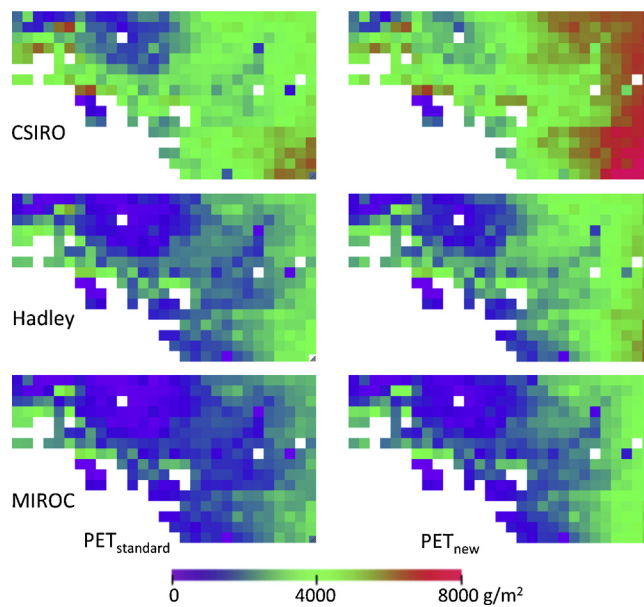


Fig. 10. Mean aboveground live tree C in 2091–2100 simulated by MC1 when fire is turned off during the 21st century for three downscaled GCM-generated future climates. Simulations on the left were generated with the standard MC1 PET algorithm (PET_{standard}) and on the right with the new algorithm (PET_{new}). Note that variables are averaged over 2091–2099 for Hadley.

We simulated two possible fire management strategies and in both cases found strong differentiation between areas of high vs. low woody encroachment, particularly with frequent fall fires, where grassland is maintained across most of the NGP in all cases (Figs. 11 and 12). This pattern occurs because trees are modeled to become more resistant to simulated fire effects as they increase in size. Frequent fires and/or unfavorable climates for growth (drought in the NGP) yield low tree biomass and hence short trees at the time of first fire, resulting in crown fires, which greatly reduce simulated tree biomass. With infrequent fires and/or favorable climates for growth, fire mortality is lower and woody encroachment is promoted.

With infrequent spring burns, the area of low woody encroachment increases substantially with the aridity of the future climate, as indicated by comparison of results for CSIRO (warm and moist), Hadley (hot) and MIROC (hot and dry) (Fig. 11). This behavior is caused by the decrease in tree biomass accumulation rates over this aridity gradient in the absence of fire (Figs. 9 and 10) and to some extent by the increase in fire intensity associated with declining fuel moisture content at time of fire. Even with frequent fires, trees in the relatively cool and moist NE corner of the NGP escape fire, but this area of woody encroachment also decreases with increasing aridity of the future climate (Fig. 12). Frequent crown fires are simulated across the rest of the NGP, thereby maintaining grasslands.

For all climates and fire scenarios, greater woody encroachment is simulated with the new PET algorithm than with the standard one, as expected, because the new algorithm simulates less water limitation of growth than does the standard one. This result derives from the fact that the scalar that modifies production as a function of water availability is proportional to (monthly plant available water)/(monthly PET), when this ratio is less than 0.8. The difference in woody encroachment derived with the two PET algorithms is of the same magnitude as the difference between that simulated for Hadley and the drier MIROC climate with the same PET algorithm across all fire management scenarios (Figs. 10–12). Although the relative effects for one future climate vs. another are similar for the two algorithms, there are substantial differences in the absolute effects simulated for a given future climate. For future climates where

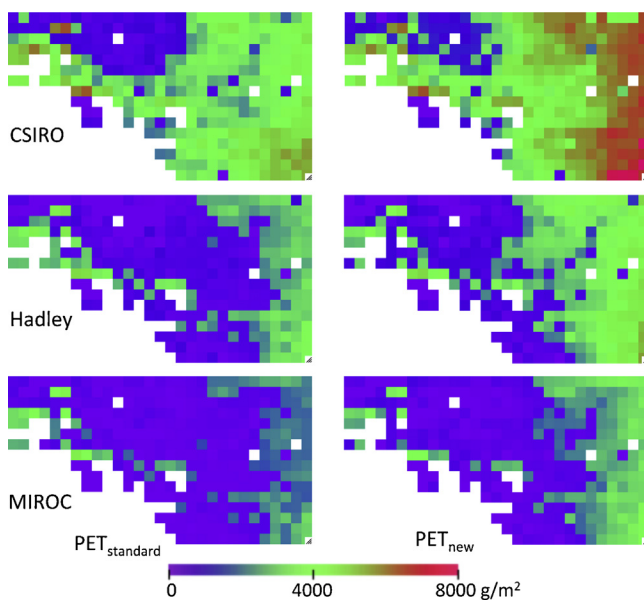


Fig. 11. Mean aboveground live tree C in 2091–2100 simulated by MC1 with spring burns every 40 years during the 21st century for three future climates. Simulations on the left generated with the standard MC1 PET algorithm ($PET_{standard}$) and on the right with the new algorithm

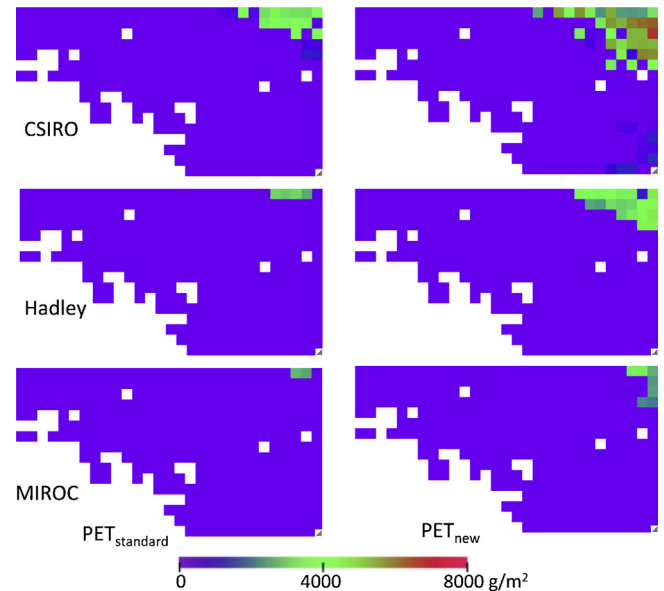


Fig. 12. Mean aboveground live-tree C in 2091–2100 simulated by MC1 with fall burns every 10 years during the 21st century for three future climates. Simulations on the left generated with the standard MC1 PET algorithm ($PET_{standard}$) and on the right with the new algorithm (PET_{new}).

precipitation and relative humidity remain the same or increase (as was the case for CSIRO) use of the new vs. standard algorithm could result in the projection of increasing rather than decreasing water resources. However, the differences in projected woody encroachment associated with differences in future climates and/or PET algorithm are modest compared to the differences associated with changes in fire frequency (Figs. 10–12). This finding is in accordance with Archer et al.'s (1995) conclusion that changes in land use have been the primary drivers of woody encroachment in the North American Great Plains.

3.4. Uncertainties

Uncertainties in our projections of vegetation include the fact that MC1 does not simulate enhanced tree mortality due to severe drought or drought–insect–pathogen interactions. In the Southwestern U.S., where recent episodes of tree mortality have been attributed in part to climate change, drought severity is projected to routinely exceed that of current once-per-thousand-year droughts by the 2050s (Williams et al., 2013). This projection is based on an empirical forest drought–stress index that involves cold-season precipitation and warm season vapor pressure deficit, but not PET. However, Williams et al. (2013) do not include increases in productivity and/or water use efficiency that may accrue from elevated CO_2 (Keenan et al., 2013; Silva and Anand, 2013), effects that are included in MC1. Thus, the improvement in the PET algorithm addressed here is only one of a number of factors requiring attention in ecological assessments of climate change impacts. For example, the effect of changes in fire regimes, both historically and in the future should also be included in projections of future vegetation dynamics (King et al., 2013a).

4. Conclusions

We developed a new PET algorithm that links surface shortwave insolation to extraterrestrial radiation via the atmospheric transmittance and then calculates net radiation as a function of shortwave insolation, temperature, and transmittance (Eq. (4) and (5)). This new estimate of net radiation was then used in place of an

estimate based solely on temperature in the Penman equation for PET. Simulation results showed that projected woody expansion across the NGP was substantially increased by this improved calculation of PET.

Our relation between transmittance and diurnal temperature range was determined for the NGP and further assessments for other regions are needed to confirm our results on a larger scale. This relation may also shift with greenhouse gas-driven warming, as may the relation between net radiation and shortwave insolation. Both of these possibilities could be assessed with analyses of GCM-derived radiation fields that are available at 3-h resolution from the most recent phase of the Coupled Model Intercomparison Project (CMIP5, Taylor et al., 2012). The full array of CMIP5 outputs could also be used to compute PET, as done by Scheff and Frierson (2014), for comparison with that generated by our algorithm. Such was not the goal of our study, which addressed a major bias in the use of temperature-based empirical estimates of PET, as shown by improved agreement with future PET projections based on more rigorous methods (Morgan et al., 2011; Scheff 2011; Scheff and Frierson 2014).

We found increasing biases in our temperature-based PET estimates that become noticeable after ~2025, as compared to those of our new algorithm (Fig. 6). The substantive differences in projected woody encroachment of the NGP by the end of the 21st century with our new vs. standard MC1 PET algorithm (Figs. 10–12) imply that algorithms based solely on temperature should be avoided for long-term ecological projections of climate change effects. The new algorithm still predicts substantial future drying for the Hadley and MIROC climates, as indicated by decreases in the ratio of annual precipitation to PET. For CSIRO this ratio decreases slightly for the standard algorithm, but increases for the new algorithm (suggesting a wetter future), as determined from the percent changes in precipitation and PET for 2081–2100 vs. 1981–2000 (Tables 2 and 4). On average, the projected trends with the new PET algorithm are consistent with the moderate level of future drying projected by Feng and Fu (2013) for the NGP based on CMIP5 data from 27 GCMs for the RCP85 scenario.

Acknowledgements

We thank Richard Waring, Joe Barsugli, Andrea Ray and David Turner for helpful comments on the manuscript. Funding was provided by the U.S. Department of Interior's North Central Climate Science Center.

References

- Allen, J.B., Crow, F.R., 1971. Predicting lake evaporation by performance of evaporation ponds, pans and tanks. *Trans. ASAE* 14, 458–463.
- Anderson, R.C., 1990. The historic role of fire in the North American grassland. In: Collins, S.L., Wallace, L.L. (Eds.), *Fire in North American Tallgrass Prairies*. University of Oklahoma Press, Norman OK, pp. 8–18.
- Archer, S.R., Schimel, D.S., Holland, E.A., 1995. Mechanisms of shrubland expansion: land use, climate or CO₂? *Clim. Change* 29, 91–99.
- Bachelet, D., Lenihan, J.M., Daly, C., Neilson, R.P., 2000. Interactions between fire, grazing and climate change at Wind Cave National Park, SD. *Ecol. Modell.* 134, 229–244.
- Bachelet, D., Lenihan, J.M., Daly, C., Neilson, R.P., Ojima, D.S., Parton, W.J., 2001. MC1. A Dynamic Vegetation Model for Estimating the Distribution of Vegetation and Associated Carbon and Nutrient Fluxes, Technical Documentation Version 1.0. General Technical Report PNW-GTR-508. USDA Forest Service. Pacific Northwest Station, Portland, OR.
- Bachelet, D., Neilson, R.P., Hickler, T., Drapek, R.J., Lenihan, J.M., Sykes, M.T., Smith, B., Stich, S., Thonicke, K., 2003. Simulating past and future dynamics of natural ecosystems in the United States. *Global Biogeochem. Cycles* 17, 1045.
- Barger, N.N., Archer, S.R., Campbell, J.L., Huang, C.y., Morton, J.A., Knapp, A.K., 2011. Woody plant proliferation in North American drylands: a synthesis of impacts on ecosystem carbon balance. *J. Geophys. Res.* 116 doi:<http://dx.doi.org/10.1029/2010JG001506> G00K07.
- Bristow, K.L., Campbell, G.S., 1984. On the relationship between incoming solar radiation and daily maximum and minimum temperature. *Agric. For. Meteorol.* 31, 159–166.
- Churkina, G., Running, S.W., Schloss, A.L., The participants of the Potsdam NPP Model Intercomparison, 1999. Comparing global models of terrestrial net primary productivity (NPP): the importance of water availability. *Global Change Biol.* 5 (Suppl. 1), 46–55.
- Courtwright, J., 2011. *Prairie Fire: A Great Plains History*. University Press of Kansas, Lawrence, KS.
- Daly, C., Halbleib, M., Smith, J.I., Gibson, W.P., Doggett, M.K., Taylor, G.H., Curtis, J., Pasteris, P.P., 2008. Physiographically sensitive mapping of climatological temperature and precipitation across the conterminous United States. *Int. J. Climatol.* 28, 2031–2064.
- de Magalhães, R.M.Q., Schwill, D.W., 2012. Leaf traits and litter flammability: evidence for non-additive mixture effects in a temperate forest. *J. Ecol.* 100, 1153–1163.
- Eagleman, J.R., 1967. Pan evaporation, potential and actual evapotranspiration. *J. Appl. Meteorol.* 6, 482–488.
- Eggemeyer, K.D., Awada, T., Wedin, D.A., Harvey, F.E., Zhou, X., 2006. Ecophysiology of two native invasive woody species and two dominant warm-season grasses in the semiarid grasslands of the Nebraska Sandhills. *Int. J. Plant Sci.* 16, 991–999.
- Feng, S., Fu, Q., 2013. Expansion of global drylands under a warming climate. *Atmos. Chem. Phys.* 13, 10081–10094.
- Fisher, J.B., Whittaker, R.J., Malhi, Y., 2011. ET come home: potential evapotranspiration in geographical ecology. *Global Ecol. Biogeogr.* 20, 1–18.
- Fowler, H.J., Blenkinsop, S., Tebaldi, C., 2007. Linking climate change modeling to impacts studies: recent advances in downscaling techniques for hydrological modeling. *Int. J. Climatol.* 27, 1547–1578.
- Fuhlendorf, S.D., Smeins, F.E., Grant, W.E., 1996. Simulation of a fire-sensitive ecological threshold: a case study of Ashe juniper on the Edwards Plateau of Texas, USA. *Ecol. Modell.* 90, 245–255.
- Gordon, H.B., 2002. The CSIRO Mk3 Climate System Model. CSIRO Atmospheric Research Technical Paper 60. CSIRO, Aspendale, Victoria Australia.
- Gray, L.K., Hamann, A., 2013. Tracking suitable habitat for tree populations under climate change in western North America. *Clim. Change* 117, 289–303.
- Gustafson, E.J., Sturtevant, B.R., 2013. Modeling forest mortality caused by drought stress: implications for climate change. *Ecosystems* 16, 60–74.
- Guttman, N.B., 1998. Comparing the Palmer Drought Index and the Standardized Precipitation Index. *JAWRA J. Am. Water Resour. Assoc.* 34, 113–121.
- Halofsky, J.E., Hemstrom, M.A., Conklin, D.R., Halofsky, J.S., Kerns, B.K., Bachelet, D., 2013. Assessing potential climate change effects on vegetation using a linked model approach. *Ecol. Modell.* 266, 131–143.
- Hamon, W.R., 1961. Estimating potential evapotranspiration. *J. Hydr. Div. Proc. ASCE* 87 HYC 107–120.
- K-1 Coupled Model (MIROC) Description. Technical Report 1. In: Hasumi, H., Emori, S. (Eds.), University of Tokyo, Center for Climate System Research, Tokyo.
- Higgins, K.F., 1986. Interpretation and Compendium of Historical Fire Accounts in the Northern Great Plains. Resource Publication 161. U. S. Fish and Wildlife Service, Washington DC.
- Hobbins, M.T., Dai, A., Roderick, M.L., Farquhar, G.D., 2008. Revisiting the parameterization of potential evaporation as a driver of long-term water balance trends. *Geophys. Res. Lett.* 35 doi:<http://dx.doi.org/10.1029/2008GL033840> L12403.
- Hobbins, M., Wood, A., Streubel, D., Werner, K., 2012. What drives the variability of evaporative demand across the conterminous United States? *J. Hydrometeorol.* 13, 1195–1214.
- Holecheck, J.L., Gomez, H., Molinar, F., Galt, D., 1999. Grazing studies: what we've learned. *Rangelands* 21 (2), 12–16.
- Howell, T.A., Evett, S.R., 2006. The Penman–Monteith Method. Available on-line: <http://www.cprl.ars.usda.gov/wmru/pdfs/PM%20COLO%20Bar%202004%20corrected%209apr04.pdf> (verified: 23.08.13).
- IPCC [Intergovernmental Panel on Climate Change], 2007. *Climate Change 2007: The Physical Science Basis. Contribution of Working Group I to the Fourth Assessment Report of the Intergovernmental Panel on Climate Change*. In: Solomon, S., Qin, D., Manning, M., Chen, Z., Marquis, M., Avery, K.B., Tignor, M., Miller, H.L. (Eds.), Cambridge University Press, Cambridge and New York.
- Jensen, M.E., Burman, R.D., Allen, R.G., 1990. *Evapotranspiration and Irrigation Water Requirements*. ASCE Manuals and Reports on Engineering Practices No. 70. ASCE, Reston, VA.
- Johns, T.C., Gregory, J.M., Ingram, W.J., Johnson, C.E., Jones, A., Lowe, J.A., Mitchell, J.F. B., Roberts, D.L., Sexton, D.M.H., Stevenson, D.S., Tett, S.F.B., Woddage, M.J., 2003. Anthropogenic climate change for 1860 to 2100 simulated with the HadCM3 model under updated emissions scenarios. *Clim. Dyn.* 20, 583–612.
- Keenan, T.F., Hollinger, D.Y., Bohrer, G., Dragoni, D., Munger, J.W., Schmid, H.P., Richardson, A.D., 2013. Increase in forest water-use efficiency as atmospheric carbon dioxide concentrations rise. *Nature* 499, 324–328.
- Kern, J.S., 1995. Geographic patterns of soils water-holding capacity in the contiguous United States. *Soil Sci. Soc. Am.* 59, 1126–1133.
- Kern, J.S., 2000. Erratum for Geographic patterns of soils water-holding capacity in the contiguous United States. *Soil Sci. Soc. Am.* 64, 382.
- King, D.A., Bachelet, D.M., Symstad, A.J., 2013a. Climate change and fire effects on a prairie-woodland ecotone: projecting species range shifts with a dynamic global vegetation model. *Ecol. Evol.* 3, 5076–5097.
- King, D.A., Bachelet, D.M., Symstad, A.J., 2013. *Vegetation projections for Wind Cave National Park with three future climate scenarios: Final report in completion of*

- task agreement J8W07100052. Natural Resource Technical Report NPS/WICA/NRTR – 2013/681.
- Küchler, A., 1975. Potential Natural Vegetation of the United States, 2nd ed. American Geographical Society, New York.
- Lenihan, J.M., Bachelet, D., Neilson, R.P., Drapek, R.J., 2008. Simulated response of conterminous United States ecosystems to climate change at different levels of fire suppression, CO₂ emission rate, and growth response to CO₂. *Global Planet. Change* 64, 16–25.
- Linacre, E.T., 1967. Climate and the evaporation from crops. *J. Irrig. Drain. Div. Proc. ASCE* 93 (4), 61–79.
- Linacre, E.T., 1968. Estimating the net-radiation flux. *Agric. Meteorol.* 5, 49–63.
- Linacre, E.T., 1977. A simple formula for estimating evaporation rates in various climates, using temperature data alone. *Agric. Meteorol.* 18, 409–424.
- Littell, J.S., Oneil, E.E., McKenzie, D., Hicke, J.A., Lutz, J.A., Norheim, R.A., Elsner, M.M., 2010. Forest ecosystems, disturbance, and climatic change in Washington State, USA. *Clim. Change* 102, 129–158.
- Lu, J., Sun, G., McNulty, S.G., Amaty, D.M., 2005. A comparison of six potential evapotranspiration methods for regional use in the Southeastern United States. *J. Am. Water Resour. Assoc.* 41, 621–633.
- Lutes, D.C., Robinson, D.C.E., 2003. Variant descriptions. In: Reinhardt, E., Crookston, N.L. (Eds.), *The Fire and Fuels Extension to the Forest Vegetation Simulator*. General Technical Report RMRS-GTR-116. USDA Forest Service, Rocky Mountain Research Station, Ogden, UT (chapter 4).
- Milly, P.C.D., Dunne, K.A., 2011. On the hydrologic adjustment of climate-model projections: the potential pitfall of potential evapotranspiration. *Earth Interact.* 15 Paper 15-001.
- Mitchell, K.E., Lohmann, D., Houser, P.R., Wood, E.F., Schaake, J.C., Robock, A., Cosgrove, B.A., Sheffield, J., Duan, Q., Luo, L., Higgins, R.W., Pinker, R.T., Tarpley, J.D., Lettenmaier, D.P., Marshall, C.H., Entin, J.K., Pan, M., Shi, W., Koren, V., Meng, J., Ramsay, B.H., Bailey, A.A., 2004. The multi-institution North American Land Data Assimilation System (NLDAS): utilizing multiple GCM products and partners in a continental distributed hydrological modeling system. *J. Geophys. Res.* 109 doi:http://dx.doi.org/10.1029/2003JD003823 D07S90.
- Monteith, J.L., 1965. Evaporation and environment. In: Fogg, G.E. (Ed.), *Symposia of the Society for Experimental Biology: The State and Movement of Water in Living Organisms*, vol. 19. Academic Press, New York, pp. 205–234.
- Morgan, J.A., LeCain, D.R., Pendall, E., Blumenthal, D.M., Kimball, B.A., Carrillo, Y., Williams, D.G., Heisler-White, J., Dijkstra, F.A., West, M., 2011. C4 grasses prosper as carbon dioxide eliminates desiccation in warmed semi-arid grassland. *Nature* 476, 202–206.
- Special Report on Emissions Scenarios. A Special Report of Working Group III of the Intergovernmental Panel on Climate Change. In: Nakićenović, N., Swart, R. (Eds.), Cambridge University Press, Cambridge and New York.
- Norris, M.D., Blair, J.M., Johnson, L.C., McKane, R.B., 2001. Assessing changes in biomass, productivity, and C and N stores following *Juniperus virginiana* forest expansion into tallgrass prairie. *Can. J. For. Res.* 31, 1940–1946.
- NREL (National Renewable Energy Laboratory), 1993. Solar and Meteorological Surface Observation Network, 1961–1990. U.S. Department of Energy, National Renewable Energy Laboratory, Golden, CO.
- Olson, D.M., Dinerstein, E., 2002. The global 200: priority ecoregions for global conservation. *Ann. Missouri Bot. Gard.* 89, 199–224.
- Penman, H.L., 1948. Natural evaporation from open water, bare soil, and grass. *Proc. R. Soc. London. Ser. A* 193 (1032), 120–146.
- Rao, L.Y., Sun, G., Ford, C.R., Vose, J.M., 2011. Modeling potential evapotranspiration of two forested watersheds in the Southern Appalachians. *Trans. ASABE* 54, 2067–2078.
- Rogers, B.M., Neilson, R.P., Drapek, R., Lenihan, J.M., Wells, J.R., Bachelet, D., Law, B.E., 2011. Impacts of climate change on fire regimes and carbon stocks of the U.S. Pacific Northwest. *J. Geophys. Res.* 116 doi:http://dx.doi.org/10.1029/2011JG001695 G03037.
- Roderick, M.L., Hobbins, M.T., Farquhar, G.D., 2009. Pan evaporation trends and the terrestrial water balance I. Principles and observations. *Geogr. Compass* 3 (2), 746–760. doi:http://dx.doi.org/10.1111/j.1749-8198.2008.00213.x.
- Rotstayn, L.D., Roderick, M.L., Farquhar, G.D., 2006. A simple pan-evaporation model for analysis of climate simulations: evaluation over Australia. *Geophys. Res. Lett.* 33, L17715. doi:http://dx.doi.org/10.1029/2006GL027114.
- Samson, F.B., Knopf, F.L., Ostlie, W.R., 1998. Grasslands. In: Mac, M.J., Opler, P.A., Puckett Haecker, C.E., Doran, P.D. (Eds.), *Status and Trends of the Nation's Biological Resources*. U.S. Department of the Interior, U.S. Geological Survey, Washington DC, pp. 437–472.
- Scheff, J. 2011. Reference evapotranspiration from standard archived GCM output: a proof of concept. www.atmos.washington.edu/~jack/PotEvapGCM.ps.
- Scheff, J., Frierson, D.M., 2014. Scaling potential evapotranspiration with greenhouse warming. *J. Clim.* 27, 1539–1558. <http://dx.doi.org/10.1175/JCLI-D-13-00233.1>.
- Sheffield, J., Wood, E.F., Roderick, M.L., 2012. Little change in global drought over the past 60 years. *Nature* 491, 435–438. doi:http://dx.doi.org/10.1038/nature11575.
- Silva, L.C.R., Anand, M., 2013. Probing for the influence of atmospheric CO₂ and climate change on forest ecosystems across biomes. *Global Ecol. Biogeogr.* 22, 83–92.
- Spencer, C.N., Matzner, S.L., Smalley, J., Bukrey, M., Onberg, J., Chapman, M., Steck, M., 2009. Forest expansion and soil carbon changes in the Loess Hills of eastern South Dakota. *Am. Midl. Nat.* 161, 273–285.
- Spitters, C.J.T., Toussaint, H.A.J.M., Goudriaan, J., 1986. Separating the diffuse and direct component of global radiation and its implications for modeling canopy photosynthesis Part I. Components of incoming radiation. *Agric. Forest Meteorol.* 38, 217–229.
- Sud, Y.C., Mocko, D.M., Lau, K.-M., Atlas, R., 2003. Simulating the Midwestern U.S. drought of 1988 with a GCM. *J. Clim.* 16, 3946–3965.
- Taylor, K.E., Stouffer, R.J., Meehl, G.A., 2012. An overview of CMIP5 and the experiment design. *Bull. Am. Meteorol. Soc.* 93, 485–498.
- Thornton, C.W., 1948. An approach toward a rational classification of climate. *Geogr. Rev.* 38, 55–94.
- Thornton, P.E., Running, S.W., 1999. An improved algorithm for estimating incident daily solar radiation from measurements of temperature, humidity, and precipitation. *Agric. Forest Meteorol.* 93, 211–228.
- Williams, A.P., Allen, C.D., Macalady, A.K., Griffin, D., Woodhouse, C.A., Meko, D.M., Grissino-Mayer, H.D., Dean, J.S., Cook, E.R., Gangodagamage, C., Cai, M., McDowell, N.G., 2013. Temperature as a potent driver of regional forest drought stress and tree mortality. *Nat. Clim. Change* 3, 292–297.